Highly efficient biosorbent produced from Syagrus romanzoffiana to be applied in water treatment

Gabriel André Tochetto (tochettogabriel@gmail.com)
Federal University of Santa Catarina: Universidade Federal de Santa Catarina https://orcid.org/0000-0003-1656-505X
Tainá Cristini da Silva
UFFS: Universidade Federal da Fronteira Sul
Josiane Bampi
UFFS: Universidade Federal da Fronteira Sul
Regina de Fátima Peralta Muniz Moreira
Federal University of Santa Catarina: Universidade Federal de Santa Catarina
Cleuzir da Luz
UDESC: Universidade do Estado de Santa Catarina
Gean Delise Leal Pasquali
UFFS: Universidade Federal da Fronteira Sul
Adriana Dervanoski
UFFS: Universidade Federal da Fronteira Sul

Research Article

Keywords: Adsorption, Methylene blue, Jerivá coconut, Nonlinear fitting

Posted Date: November 4th, 2021

DOI: https://doi.org/10.21203/rs.3.rs-996508/v1

Abstract

A new adsorbent from Jerivá coconut (a native fruit of the Atlantic Forest) was developed through thermal activation at high temperatures and chemical activation using H_3PO_4. The characterization of activated carbon revealed the functional groups O-H, NH_2 and C=C. The morphology showed an irregular and heterogeneous surface, with a pore volume of 0.442 $cm^3\ g^{-1}$ and a surface area of 750 $m^2\ g^{-1}$. The main variables of the process were evaluated for statistical significance in the removal of the methylene blue dye showing that only the agitation of the system affected the process. Adsorption kinetics were performed at three different concentrations and fitted to nonlinear models where the Avrami-fractional-order model represented the experimental data. Equilibrium occurred within 80 min and was sufficient to remove more than 99% of the initial concentration. The sorption isotherms were performed at four different temperatures, fitted to four nonlinear models. The Sips model obtained the best adjustment, with a maximum adsorption capacity of 254.40 mg g^{-1}, for the highest temperature investigated. The process occurred spontaneously, favorably and endothermically. The results were promising, pointing out that this adsorbent has the potential to remove methylene blue and the treated effluent can be reused for less noble purposes in the industry.

1. Introduction

Coconut shell is one of the main lignocellulosic sources for the production of activated carbon (AC), since in Brazil there are about 280 thousand hectares of planted palm trees. The Jerivá coconut is a fruit obtained from a palm tree (*Syagrus romanzoffiana*) originating from the Atlantic Forest, which is distributed throughout South America (Falasca et al. 2012), tolerates temperature variations, but grows better in a tropical climate (Moreira et al. 2013). This biomass, after thermal and chemical treatments, has the potential to be used as an adsorbent applied to water treatment. Recently, the use of activated carbon produced from this biomass has been reported in the removal of metallic ions (Pigatto et al. 2020), herbicides (Salomón et al. 2021) or antibiotics (Carvalho et al. 2019) dissolved in the aqueous phase. The results of the studies were promising and, therefore, the evaluation of this new adsorbent in the separation of other contaminants in the aqueous phase and the understanding of the mechanisms involved is of great scientific and technological interest.

The characteristics of an adsorbent can be enhanced through physical or chemical activation (Selmi et al. 2021), modifying the structure and even the composition of the material. While the physical activation process results from the oxidation of carbonaceous material, in the chemical activation route, dehydrating agents are impregnated into the material and calcined (Danish et al. 2018). Phosphoric acid, potassium hydroxide and zinc chloride are widely used as impregnating agents for the development of microporous and high surface area adsorbents (Molina-Sabio and Rodríguez-Reinoso 2004).

The ideal activated carbon must have a high volume of micropores, but also have meso and macropores of different sizes, allowing it to adsorb a wide range of molecules. Activation with $ZnCl_2$ induces the production of micropores with uniform distribution, while impregnation with H_3PO_4 leads to the

development of heterogeneous micropores, therefore, with a wide pore size distribution (Molina-Sabio and Rodríguez-Reinoso 2004). Some authors have reported this behavior, that H_3PO_4 is more suitable for modifying the structure of lignocellulosic material, producing greater pore size distribution and high surface areas (Pintor et al. 2013; Danish et al. 2018).

Thus, the objective of this study was to obtain an adsorbent with high surface area and pore volume from activation with H_3PO_4 combined with high temperatures, evaluate the efficiency of methylene blue removal and understand through kinetic and thermodynamic studies the mechanisms involved in the mass transfer process.

2. Materials And Methods

2.1 Chemicals and materials

The precursor material used to develop the adsorbent is Jerivá coconut, harvested during the green phase of the *Syagrus romanzoffiana* plant, in the state of RS, Brazil. The characteristics of this biomass have already been investigated in other works (Coimbra and Jorge 2011; Moreira et al. 2013; Pigatto et al. 2020). The activating agent used was phosphoric acid (H_3PO_4) at a concentration of 40%. Deionized water was used to prepare the solutions.

To evaluate the adsorptive capacity of charcoal produced from Jerivá coconut, kinetic and thermodynamic studies were carried out using an aqueous solution containing methylene blue (MB- $C_{16}H_{18}ClN_3S$), a non-biodegradable aromatic heterocyclic compound with cationic characteristics and high solubility in water (43.6 g L^{-1} at 25°C). It has a molar mass of 319.85 g mol^{-1}, a molecular diameter of 0.8 nm and a pKa of 3.14 (NCBI, 2020). This dye was chosen because it is considered a model molecule (Liu et al. 2012) that presents strong sorption on solids with anionic characteristics (Doğan et al. 2004) and is extensively used for this purpose. For pH adjustment, solutions of sodium hydroxide (NaOH) and hydrochloric acid (HCl) were used at concentrations of 0.1 M.

2.2 Development and activation of the Jerivá carbon

Aiming to produce an efficient adsorbent, but respecting the principles of green engineering (Anastas and Zimmerman 2003), all parts of the Jerivá coconut (epicarp, mesocarp and endocarp) were used. It was dried in an oven (Solab, SL-100) for 72 h at 80 ± 1°C, in order to remove moisture from the material, after which it was ground to reduce the granulometry until obtaining a bran. Jerivá coconut bran was soaked in a 1:1 H_3PO_4 solution, the mixture was homogenized and dehydrated for 15 h in an oven at 105 ± 1°C. The material was calcined in a muffle oven (Lavoisier, 400 D) at 600 ± 5°C and held for 30 minutes after the oven reached the desired temperature (Basu et al. 2018). The adsorbent material was called activated carbon of Jerivá coconut (ACJC).

2.3 Characterization of activated carbon of Jerivá coconut

The characterization of activated carbon produced from Jerivá coconut (ACJC) was performed by determining oxygenated functionalities using the Fourier Transform Infrared Spectroscopy (FTIR, Shimatzu, IRTracer-100) technique. The morphology of the adsorbent was observed through a Scanning Electron Microscopy (SEM) (Leica, ATC 2000), the particles were dispersed in carbon ribbon and coated with gold. A spot semi-quantitative chemical analysis was also performed using Energy Dispersive Spectroscopy (EDS). The specific area of the ACJC was determined by nitrogen isotherm at 77 K in a Surface Analyzer (QuantaChrome, Nova 1200e). Applying the equation proposed by BET (Brunauer et al. 1938) to the sorption isotherm obtained, the surface area (S_{BET}) was calculated. Total pore volume (T_{PV}) was calculated by a method developed by BJH (Barrett et al. 1951).

2.4 Effect of finite bath adsorption operating conditions on adsorption capacity.

MB removal was studied through the experimental design of the Plackett-Burman type, in order to evaluate which of the variables (pH, dye concentration, agitation, system temperature, and adsorbent mass) affect the sorption process using the ACJC. Each of the variables was evaluated at three levels (-1, 0, +1), with 16 tests, using 4 central points. The complete matrix can be found in Table SM1.

2.5 Sorption Kinetics

The MB sorption kinetics were performed with the solution's natural pH (5.85 ± 0.20) and a dosage of 5 g L^{-1} of ACJC, conditions obtained from the experimental design tests. The batch system was constantly agitated at 150 ± 1 rpm. Three concentrations were evaluated in this study (50 ± 1.4 mg L^{-1}, 75 ± 2.1 mg L^{-1} and 105 ± 1.5 mg L^{-1}). A 0.5 mL aliquot of the solution was collected at regular time intervals with a micropipette for spectrophotometric analysis. The tests were carried out with 3 h of solid-liquid contact (time required for complete dye removal). The amount of adsorbed dye q_e (mg g^{-1}) was determined by a mass balance. Nonlinear Avrami fractional-order (Lopes et al. 2003), Elovich (Pérez-Marín et al. 2007), Pseudo-first-order (Lagergreen 1898), Pseudo-second-order (Ho and McKay 1998) kinetic models were used to adjust the experimental data. The diffusion of MB in the ACJC pores was investigated using the intraparticle diffusion model (Weber and Morris 1963). All equations are described in Table SM2.

2.6 Sorption Isotherms

The thermodynamic equilibrium study between the adsorbent and the adsorbate was carried out in a batch reactor using a dose of 5 g L^{-1} and maintaining the natural pH of 5.85 ± 0.20 at different concentrations of MB, ranging from 175 to 915 ± 1.83 mg L^{-1}. The system was constantly agitated at 150 ± 1 rpm at four different temperatures (15, 25, 35 and 45 ± 1°C) for 80 min (time needed to reach equilibrium and also to prevent desorption of the contaminant after filling the sites active). The nonlinear equilibrium models of BET (Brunauer et al. 1938), Langmuir (Langmuir 1918), Freundlich (Freundlich 1906) and Sips (Sips 1950), presented in Table SM2, were fitted to the experimental results. The thermodynamic analysis was performed using the Van't Hoff graph, in order to obtain the values referring to the Gibbs free energy (ΔG^o), the enthalpy (ΔH^o) and entropy (ΔS^o) of the system.

2.7 Photometric, statistical and non-linear regression analysis

The initial and final concentrations of adsorbate were determined by the direct photometric method UV-VIS (λ = 665 nm) in a spectrophotometer (Nova instruments, Serie 1800). For all analyses, three readings were taken from each sample and an arithmetic mean of the absorbances was taken to calculate the concentration.

The results of the experimental planning were obtained through the methodology of planning and analysis of experiment of the Statistica 12.0 software (StatSoft, Germany), and the answers were analyzed through the Analysis of Variance (ANOVA). The parameters of the models that describe the kinetic and thermodynamic equilibrium behavior were fitted by non-linear regression using Matlab R2019a software (MathWorks Inc, USA). The analysis of the best adjustment of the mathematical models was given by the highest correlation coefficients (R^2) and adjusted correlation (R^2_{adj}) and lowest error values between the experimental and calculated values based on the sum of squared errors (SSE) and hybrid fractional error function (HYBRID). The equations are shown in Table SM2.

3. Results And Discussion

3.1 Characterization of activated carbon of Jerivá coconut

Vegetable-derived adsorbents are widely used to remove dyes (Sellaoui et al. 2020) as they are materials that contain functional groups that can influence and favor the sorption of organic compounds, such as MB. Thus, the surface functional groups of the ACJC were identified by the FTIR spectrum (Fig. 1). In the region of 3800-2700 cm^{-1} the highest frequencies of the hydroxyl group (O-H) are found, so the stretch at 3421 cm^{-1} can be attributed to this group (Deng et al. 2010; de Costa et al. 2015; Gupta et al. 2018; dias Júnior et al. 2019). The O-H group, in plant materials (such as coconut fiber), is related to cellulose, hemicellulose and lignin (Sreekala et al. 1997; Setiabudi et al. 2016; Gupta et al. 2018). It is also possible to infer the presence of the amino group (NH_2) with absorptions also in the range of 3200-3600 cm^{-1} (Yuvaraja et al. 2014), thus suggesting the overlapping of two bands in this region. It should be noted that the amino and hydroxyl groups have adsorptive characteristics (Tang et al. 2019), corroborating the result obtained by the N_2 isotherms, which point to chemisorption (Ruthven 1984). The high intensity band around 1600 cm^{-1} can be attributed to the vibration of the C=C groups of the aromatic rings. This band can show the presence of lignin and also the formation of aromatic compounds originated by the elimination of hydrogen and oxygen from aliphatic compounds during pyrolysis, and can provide information regarding the stretching of the C=C bond constituting the aromatic benzene molecules or rings in lignin, typical of carbonaceous material (de Sales et al. 2015; dias Júnior et al. 2019). There may also be the presence of the nitro group, since it is found in the absorption peaks of 1600-1530 cm^{-1} and 1390-1300 cm^{-1}. The appearance of peaks at 1178 and 1085 cm^{-1} may originate from the phosphorus

functional groups, resulting from the use of H_3PO_4 as an activated agent (Pan et al. 2019). Bands with values <1000 cm^{-1} are related to constituents present in wood, such as cellulose and lignin, which are eliminated at the activation temperature (600°C) (Lammers et al. 2009; Özgenç et al. 2017). Chemical modification of the carbon structure by H_3PO_4 and calcination may have enhanced the adsorptive properties (Luo et al. 2018; Tang et al. 2019).

The SEM allowed the study of the structural and morphological characteristics of activated carbon, such as the existence of pores and chemical composition. In Fig. 2a, the micrographs at 70x magnification of the ACJC are shown, where it is observed that the surface has a very irregular, rough and heterogeneous topography when it comes to the size of the grains. At 5000x magnification (Fig. 2b) the presence of a large volume of well-defined pores can be seen. These results are similar to those found in other studies, which developed carbons activated with $ZnCl_2$ from Jerivá coconut (Carvalho et al. 2019; Salomón et al. 2021). Pigatto et al. (2020) also synthesized an adsorbent material having the Jerivá coconut as precursor material, however, there was no chemical activation, only calcination, when analyzing the SEM, it is clear that the surface is rough and irregular, but it is not possible to observe the presence of pores so well structured. Thus, it can be inferred that calcination was responsible for evaporating/degrading the phosphoric acid that was impregnated in the Jerivá coconut, leaving the space that was previously occupied by the chemical reagent, resulting in the opening of pores (Deng et al. 2010; Enniya et al. 2018).

Through dispersive X-ray analysis (EDS) it was possible to identify the main elements present in an ACJC sample. It is observed that the impregnation of phosphoric acid in the adsorbent was efficient, with a significant P peak at 2 keV. It was also identified the presence of C and O at 0.3 and 0.5 keV, which can influence the sorption properties, increasing the surface polarity (Barrer 1966). The presence of C, P and O was also obtained in the study by Basu et al. (2018) which performed chemical activation with H_3PO_4. In addition to sodium, iron, potassium, calcium and tungsten in smaller amounts on the surface. SEM micrographs and EDS analysis can be viewed in Fig. SM1.

Figure 3 shows the nitrogen adsorption/desorption isotherm and the pore size distribution. According to the IUPAC, the isotherm can be classified as type I (Ruthven 1984; Thommes et al. 2015; Thi et al. 2020), since there is no hysteresis between the curves, indicating a monoatomic approximation to a limit in the adsorption capacity that corresponds to the formation of a complete layer. Usually, this type of isotherm is found in microporous adsorbates that act by chemisorption (Thi et al. 2020). The N_2 isotherm of the Jerivá coconut adsorbent developed by Salomón et al. (2021) obtained a similar result to the ACJC.

Using the N_2 isotherm, the surface area, pore volume, and average pore size were calculated (Table 1) and the values were compared to those reported in the literature using this biomass. The chemical activation with H_3PO_4 combined with high temperature was responsible for an increase of almost 700% in the surface area of the adsorbent when compared to the thermal treatment without the addition of an activating agent (Pigatto et al. 2020). The largest surface area and pore volume of the adsorbent activated with $ZnCl_2$ and produced by Carvalho et al. (2019) can be attributed to the calcination

conditions, since the firing temperature was 450°C, while in the present study 600°C was used and Salomón et al. (2021) 700°C, suggesting that lower carbonization temperatures are more indicated.

Table 1
Texture characterization of activated carbons produced from Jerivá coconut

Activating agent	S_{BET} (m^2 g^{-1})	T_{PV} (cm^3 g^{-1})	Average pore size (nm)	Reference
H_3PO_4	750	0.442	2.36	This work
$ZnCl_2$	1435	0.876	-	Carvalho et al. (2019)
$ZnCl_2$	782	0.441	2.26	Salomón et al. (2021)
-	108	0.090	-	Pigatto et al. (2020)

The relationship between the size of the adsorbate molecule with the pores can influence the diffusion mechanisms, in the case of macropores, size differences are favored, since the radius of the dye molecule is much smaller than the average pore size (Nascimento et al. 2014). In the case of micropores, they are often attributed as the main contributors to the greater sorption capacity of small molecules, such as MB, which has a molecular diameter of 0.8 nm. According to Barton (1987), a pore diameter of the order of 1.3 nm is necessary for effective sorption, so the results of the specific surface characterization allow us to infer that the adsorbent is capable of retaining the contaminant in the micropores, macropores and on the surface of the developed material.

3.2 Experimental design

Many works in the literature carry out an isolated evaluation of each variable in order to obtain the best conditions for the sorption process (Basu et al. 2018; Othman et al. 2018; Calimli et al. 2020), however, when one parameter is fixed and the others vary, it is not possible to evaluate the interaction of the variables. Thus, experimental planning allows optimizing processes by performing an interaction of all variables at the same time and obtaining results with statistical significance. The effects of the studied variables on MB removal using ACJC were evaluated using the Pareto graph (Fig. SM2). It was possible to observe that agitation was the only statistically significant variable (+4.7415), so that the increase in agitation favors dye sorption. The agitation is a factor that interferes directly in the liquid-solid sorption (Ruthven 1984), the higher the speed with which the reactor is agitated the higher the mass transfer rate and the lower the resistance that the MB molecules will find to move to the adsorbent surface, this behavior is expected since the mass transfer coefficient in the external film (k_f) is the inverse of the resistance (Nascimento et al. 2014; Cremasco 2015). The other variables were not significant, being possible to reduce operating costs, using a lower adsorbent dosage, higher dye concentrations, the aqueous solution does not need pH adjustment and room temperature can be used. These conclusions are fundamental to improve the process to minimize resources and energy consumption, thus meeting the third and fourth principles of green engineering (Anastas and Zimmerman 2003).

3.3 Mechanism of MB adsorption kinetics on ACJC

The kinetic study was carried out in order to determine the mass transfer mechanisms that control MB sorption in the ACJC. Four kinetic models were evaluated, such as fractional order Avrami, Elovich, Pseudo-first-order and Pseudo-second-order, and the parameters obtained are described in Table 2. It can be seen that the Avrami-fractional-order model obtained good adjustments to the experimental data, presenting high R^2 (> 0.990) and R^2_{adj} (> 0.988) and the lowest error values, SSE (< 0.385) and HYBRID (< 0.316), for the three concentrations studied, indicating that the Avrami model is able to adequately represent the experimental results. Thus, the calculated value of q_e predicted by the equation is very close to the value obtained experimentally.

Avrami's kinetic model has a wide application in studies involving the adsorption of dyes on activated carbons (Alencar et al. 2012; Adebayo et al. 2014; Lima et al. 2016), precisely for being able to adapt to different systems, not fixing a single kinetic order (n_{AV}) (Lima et al. 2015). As mentioned before, q_e indicates the sorption capacity of MB in ACJC, while the parameter n_{AV} is associated with possible potential changes in the adsorption mechanism (Liu and Liu 2008; Lima et al. 2016), allowing many kinetic orders to describe the adsorption process over time.

Table 2
Kinetic parameters for adsorption of MB on ACJC in different concentrations.

	51.4 mg L^{-1}	**77.1 mg L^{-1}**	**103.5 mg L^{-1}**
Experimental data			
q_e (mg g^{-1})	10.26	15.40	20.67
Avrami fractional-order			
q_e (mg g^{-1})	10.52	15.58	21.19
k_{AV} (min^{-1})	0.3316	0.4851	0.5497
n_{AV}	0.5490	0.5295	0.4231
R^2	0.9898	0.9965	0.9953
R^2_{adj}	0.9880	0.9958	0.9944
SSE	0.3062	0.2583	0.3855
HYBIRD	0.3166	0.0796	0.0797
Elovich			
α (mg (g^{-1} min^{-1}))	15.81	121.60	188.60
β (mg g^{-1})	0.6595	0.5482	0.4253
R^2	0.9608	0.9541	0.9756
R^2_{adj}	0.9536	0.9457	0.9712
SSE	0.5989	0.9541	0.8753
HYBRID	0.5211	0.9457	0.2671
Pseudo-first-order			
q_e (mg g^{-1})	9.88	14.86	19.41
k_1 (min^{-1})	0.1538	0.2622	0.2830
R^2	0.9481	0.9514	0.9141
R^2_{adj}	0.9387	0.9426	0.8985
SSE	0.7925	1.0510	1.7776

	51.4 mg L^{-1}	77.1 mg L^{-1}	103.5 mg L^{-1}
HYBRID	3.3843	1.8985	2.3723
Pseudo-second-order			
q_e (mg g^{-1})	10.61	15.71	20.54
k_2 (g mg^{-1} min^{-1})	0.0232	0.0293	0.0242
R^2	0.9735	0.9850	0.9705
R^2_{adj}	0.9686	0.9823	0.9652
SSE	0.5159	0.5423	0.9867
HYBRID	1.4498	0.5028	0.7728

Through the results obtained, an increase in the rate (k_{AV}) of dye sorption to the surface of the adsorbent is observed as the concentration increases, ranging from 0.3316 min^{-1} to 0.5497 min^{-1}. This occurred because the driving force is directly related to the increase in concentration, providing an increase in the mass transfer potential (Feng et al. 2011). In Fig. 4, the kinetic results obtained experimentally and the adjustment are presented. It is verified that the sorption was extremely fast and the amount of MB adsorbed increases in higher concentrations of the solute, however, when there is no more significant variation in the mass transfer, the equilibrium of the process is reached (Thi et al. 2020). At the equilibrium time of 80 min, residual concentrations below 0.4 mg L^{-1} were obtained, which represents a removal greater than 99 % for the three concentrations studied. This result is consistent with other highly efficient adsorbents, such as *Eucalyptus* residue activated from H_3PO_4, which achieved equilibrium in 60 min (Han et al. 2020), so the equilibrium time can be considered fast compared to other adsorbents which took about 120 min (Dawood et al. 2017), 6 h (Ahmad et al. 2021). The treated water, after adsorption with ACJC, has a very high-quality level, especially when compared to separation processes by membranes (Parakala et al. 2019; Hou et al. 2020), which are highly recommended technologies for water reuse.

The study of the mass transference of the dye molecules from the fluid phase to the solid phase of the adsorbent is extremely relevant and involves the diffusion of external and internal mass and chemical reactions on the surface of the adsorbent (Prajapati and Mondal 2020). External diffusion was not evaluated because, at agitation above 150 rpm, the thickness of the film boundary layer decreases so that it can be disregarded (Wang et al. 2018). Thus, the experimental data were fitted to the intraparticle diffusion model, such as the Weber and Morris model, which assumes that the removal of adsorbate varies with the square root of time, being determinant for the velocity (Weber and Morris 1963).

According to the result shown in Figure 5, the adsorption process can be divided into three steps, following the same behavior for the three concentrations. The first zone, obtained in the first 10 minutes, corresponds to external mass transfer. A possible explanation for the higher speed (observe k_{id} for the first zone in Table SM3) and adsorption rate may be due to the presence of available sites and some surface functional groups (Feng et al. 2012), such as OH and NH_2, revealed in the characterization of the adsorbent through the FTIR. Furthermore, it is known that the external mass transfer can be affected by concentration and agitation, so that increasing the dye concentration was able to accelerate the diffusion to the solid surface (Nascimento et al. 2014). Other factors that may have contributed to the increase in adsorption speed are the pH of the solution, the particle size, and the pore size distribution.

The steeper curve suggests that the adsorption is instantaneous and that there is a strong attraction between the dye and the functional groups. The second zone was established at 40 min and according to Feng et al. (2012) can be attributed to the intraparticle diffusion process. At this stage, there is still the presence of sites available for dye sorption, although many of which have already been filled in the previous zone. The third and last zone corresponds to the equilibrium stage, where the sorption rate is much lower (observe k_{id} for the third zone in Table SM3), until it finally ceases, due to the low concentration of adsorbate in the liquid phase (Nascimento et al. 2014; Wang et al. 2018).

The parameters of the intraparticle diffusion model are shown in Table SM3, and it is possible to observe that the model had a good adjustment to the experimental data, with high R^2 (> 0.937) and R^2_{adj} (> 0.905) and low errors (SSE < 0.307 and HYBRID < 1.514). The k_{id} constant (mg g^{-1} $min^{-0.5}$) represents the rate of diffusion in the pores, while C (mg g^{-1}) is related to the thickness of the boundary layer or the resistance to mass transfer in the external liquid film. From the values found for the diffusion speed, it can be seen that they are high, especially in the first and second zone, when compared to other similar works (Kavitha and Namasivayam 2007; Karagöz et al. 2008).

The values of C increased with the increase in the initial concentrations of MB, which indicates the increase in the thickness of the boundary layer at the highest dye concentrations, while the k_{id} had the same behavior. This is because the adsorption driving force is more intense at higher concentrations (Weng et al. 2009; Feng et al. 2011). It is also possible to observe that the diffusion coefficient decreases with time, which means that the speed at which the pores are filled by the adsorbate decreases until equilibrium is reached. The value of constant C for all sorption steps was different from zero, as well as the regression curves, for both initial dye concentrations (Figure SM3), even if they were extended they will not pass through the origin. This means that some other mechanisms such as external surface sorption, adsorption equilibrium and intraparticle diffusion are involved in the process (Özcan et al. 2005; Tang et al. 2019).

3.4 Thermodynamic equilibrium study

The applicability of new adsorbents, such as Jerivá coconut, in adsorption processes depends on information related to thermodynamic equilibrium (Kebede et al. 2018), since it plays a fundamental role

in the mass transfer of the contaminant from the liquid to the solid phase (Cremasco 2015), in addition to showing whether the adsorption is feasible. The study was carried out with the objective of obtaining the adsorption capacity of ACJC at temperatures of 15, 25, 35 and 45 ± 1°C and through adjustments of the BET, Langmuir, Freundlich and Sips models, the adsorption thermodynamics was clarified. Table 3 shows the parameters of each model and the adjustment coefficients. It appears that the Sips model has higher R^2 (> 0.9511) and R^2_{adj} (> 0.9316), however the other models also obtained good fits, thus, through the error analysis between the values predicted by the model and the experimental data, note that the Sips model has lower results for SSE and HYBID, indicating that it is the model that best represents the adsorption of MB in ACJC.

Table 3
Adsorption equilibrium parameters for MB on ACJC performed in different temperatures (adsorbent dosage = 5 g L^{-1}, shaking = 150 rpm, pH_i = 5.85, pH_f = 2.44).

	15°C	25°C	35°C	45°C
BET				
q_m (mg g^{-1})	60.03	70.18	85.36	95.57
K_S (L mg^{-1})	0.3449	0.8910	1.2862	1.7985
K_L (L mg^{-1}) x10^{-4}	4.2587	3.1024	6.4955	8.0202
R^2	0.9749	0.9468	0.9871	0.9592
R^2_{adj}	0.9649	0.9255	0.9819	0.9429
SSE	4.088	7.527	4.327	8.739
HYBRID	0.566	3.305	0.964	2.586
Freundlich				
K_F (mg g^{-1}(mg $L^{-1})^{-1/n}$)	30.86	36.49	48.65	53.03
n_F	7.253	7.970	7.42	6.694
R^2	0.9801	0.9301	0.9775	0.9824
R^2_{adj}	0.9768	0.9185	0.9738	0.9795
SSE	3.221	8.597	5.110	5.346
HYBRID	0.310	1.884	1.335	0.664
Langmuir				
q_m (mg g^{-1})	66.35	79.79	94.22	106.20
K_S (L mg^{-1})	0.2537	0.7211	0.9998	1.1180
R^2	0.9553	0.9400	0.9531	0.8918
R^2_{adj}	0.9479	0.9300	0.9453	0.8738
SSE	4.834	7.951	7.383	13.575
HYBRID	0.820	3.072	0.746	4.724

	15°C	25°C	35°C	45°C
Sips				
q_m (mg g^{-1})	93.69	115.08	141.50	254.40
K_S (mg L^{-1})$^{-1/n}$	0.365	0.521	0.492	0.258
n_S	2.897	4.105	3.416	4.463
R^2	0.9856	0.9511	0.9827	0.9845
R^2_{adj}	0.9799	0.9316	0.9758	0.9784
SSE	2.583	5.849	4.225	4.729
HYBRID	0.251	1.165	0.890	0.464

In Figure 6, it can be seen that the curves were very close to the y-axis, indicating the process is extremely favorable (Ruthven 1984). The q_{max} increases from 93.69 mg g^{-1} at 15°C to 254.40 mg g^{-1} when the temperature is 45°C, indicating that the process is endothermic, that is, there is an increase in adsorption capacity with increasing temperature. This behavior is expected, since the increase in temperature provides higher rates of diffusion of dye molecules through the boundary layer, due to a decrease in the viscosity of the medium and an increase in the mobility of the adsorbate. Furthermore, this increase in adsorption capacity can be attributed to the effects of swelling on the ACJC itself (Hameed and Ahmad 2009). The Sips model is empirically based and consists of a combination of Langmuir and Freundlich isotherms, thus, when the exponent $n_S = 1$ then the model becomes similar to Langmuir, when the constant K_S is close to 0, the model approaches Freundlich (Lima et al. 2015; An et al. 2017). According to Table 2, it was observed that $n_S > 1$ and $K_S \approx 0$, indicating that adsorption occurs in multilayers on a heterogeneous surface.

In order to evaluate the adsorption efficiency of the ACJC MB, a survey of the evaluated dye concentration range (MB) and maximum adsorption capacity (q_{max}) was carried out, based on different adsorbents obtained from biomass, as shown in the Table 4. Initially, it is noticed that ACJC can be considered an adsorbent with great potential for the adsorption of dyes, such as MB, with a q_{max} higher than most of the investigated adsorbents. It is observed that adsorbents that had some type of surface modification by a chemical agent had higher q_{max}.

Table 4
Maximum adsorption capacities for MB in different biomasses as adsorbents

Adsorbents	Activator	MB (mg L^{-1})	q_{max} (mg g^{-1})	References
seeds of *Cedrela odorata* L	-	10-750	158.5	Subratti et al. (2021)
Eucalyptus sheathiana bark	-	10-100	104.2	Dawood et al. (2016)
seeds of *Cedrela odorata*	-	20-200	111.8	Babalola et al. (2016)
Pinus radiata	-	10-70	106.4	Dawood et al. (2017)
Corn cob	KOH	100-500	333.0	Medhat et al. (2021)
Peanut shell	NaOH	-	555.6	Ahmad et al. (2021)
Coconut shells	$ZnCl_2$	25-500	156.2	Yağmur and Kaya (2021)
Eucalyptus residue	H_3PO_4	-	977.0	Han et al. (2020)
Syagrus romanzoffiana	H_3PO_4	175-915	254.4	This study

Based on the equilibrium concentrations of the adsorbate and the sorption capacity of the adsorbent at different temperatures, the thermodynamic parameters were obtained, as shown in the Van't Hoff graph (Fig. SM3). Thermodynamic analysis is important to understand how a contaminant is transferred from one phase to another and how it is distributed (Mahmoodi et al. 2010). The enthalpy change (ΔH^0) was 29.99 J mol^{-1}, the positive sign of ΔH^0 indicates that the process is endothermic (Hasan et al. 2019), and the isotherms (Table 3) show that the adsorption capacity is favored by increasing temperature. Regarding the entropy variation (ΔS^0), 86.39 J mol^{-1} K^{-1} was obtained, indicating the affinity between ACJC and MB. The behavior regarding the energy flow between the system and the neighborhood, through the Gibbs free energy (ΔG^0), also indicates spontaneity in the opposite direction, since the values (-24.86 kJ mol^{-1}, -25.73 kJ mol^{-1}, -26.60 kJ mol^{-1} and -27.46 kJ mol^{-1}) are negative (Mahmoodi et al. 2010). Similar thermodynamic results were found for other adsorbents developed from *Syagrus romanzoffiana* activated with $ZnCl_2$ (Carvalho et al. 2019; Salomón et al. 2021).

3.5 MB Adsorption Mechanisms

The pH of the solution is one of the most important factors that regulate the sorption characteristics of active carbons, as the pH can change their surface charge and solute speciation (Wang and Chen 2015; Tang et al. 2019). Thus, this parameter was monitored during the kinetic and thermodynamic equilibrium tests. It was observed that the initial pH of the MB solution was 5.85 ± 0.20 and after contact with ACJC the pH decreased to 2.44 ± 0.32, this behavior being expected since the activation of the adsorbent occurred by impregnation of phosphoric acid. The activating agent was responsible for the acidic surface of the carbon and, even after washing with water and calcium carbonate, this characteristic did not

change. As the mass transfer from the liquid medium to the solid occurred under acidic conditions and the dye pKa is 3.14, it is suggested that the sorption occurred by Van der Waals interactions. Adsorbate is in protonated form when pH < pKa and deprotonated when pH > pKa (Liu et al. 2010), thus at the beginning of the sorption process, MB is presented in deprotonated form, but over time the pH decays and stabilizes at 2.44 ± 0.32 indicating that the dye is in a protonated condition in this study.

The adsorption of a certain molecule on the surface of the adsorbent can occur through different types of interactions that affect the sorption capacity (Somsesta et al. 2020). In Fig. 7, an illustration of the possible mechanisms involved has been sketched. The first mechanism that may be acting on the adsorption of MB on ACJC is the π-π stacking interaction, since the characterization of ACJC revealed the presence of functional groups characteristic of aromatic rings and the MB molecule itself is composed of these rings, suggesting a possible multilayer adsorption (Liu et al. 2011; Iwuozor et al. 2021). Adsorbents obtained from biomass have surface groups of the OH type, which can interact with the dye molecule, more specifically with nitrogen, forming a hydrogen bond (Liu et al. 2011; Somsesta et al. 2020; Iwuozor et al. 2021). Electrostatic attractions can also contribute to adsorption, since the ACJC surface has functional oxygenated groups (with more acidic and negatively charged characteristics) and MB is a cationic dye (Somsesta et al. 2020; Jawad et al. 2021).

4. Conclusion

As water availability decreases, legislation becomes more restrictive and the market demands sustainable processes, the reuse of wastewater, after treatment, becomes a necessity. The adsorbent, obtained from an abundant and low-cost biomass, such as Jerivá coconut *(Syagrus romanzoffiana*), activated at high temperatures with H_3PO_4 was effective in removing methylene blue. Treated water has potential use for reuse in less noble activities in the textile industry. The characterization of ACJC revealed morphological and structural characteristics, such as high surface area (749.80 $m^2\ g^{-1}$) compatible with commercial adsorbents. Adsorption kinetics revealed that at the equilibrium time of 80 min, removals were greater than 99%. Avrami's model proved to be more appropriate to describe the experimental results. The maximum adsorption capacity predicted by the Sips model was 254.4 mg g^{-1} for the highest temperature. The process was spontaneous, favorable and endothermic.

Declarations

Ethics approval and consent to participate

Not applicable.

Consent for publication

Not applicable.

Availability of data and materials

All datasets generated and analysed are included in this published article and its supplementary information files.

Competing interests

The authors declare that they have no competing interests.

Funding

This study received financial support from the Federal University of Fronteira Sul (UFFS, project number 1105/GR/UFFS/2018 and 1123/GR/UFFS/2018).

Author's contributions

GAT: Conceptualization, Data curation, Methodology, Formal analysis, Original Draft, Review & Editing; **TCS**: Data curation, Methodology, Original Draft, Review & Editing; **JB**: Data curation, Methodology, Original Draft, Review & Editing; **RFPMM**: Investigation, Supervision, Original Draft, Review & Editing; **CL**: Resources, Supervision, Review & Editing; **GDLP**: Conceptualization, Investigation, Resources, Supervision, Original Draft, Review & Editing; **AD**: Conceptualization, Formal analysis, Resources, Supervision, Original Draft, Review & Editing.

Acknowledgments

The authors thank the Federal University of Fronteira Sul (UFFS) for the infrastructure and support, to Financier of Studies and Projects (FINEP) for financing the structure of the analytical center of the Erechim campus and to the laboratory technicians, especially Suzana and Denys for the analyzes performed.

Nomenclature

S_{BET} (mg g^{-1})	Specific surface area
T_{PV} (cm^3 g^{-1})	Total pore volume
q_e (mg g^{-1})	Amount of adsorbate adsorbed
q_{max} (mg g^{-1})	Maximum amount of adsorption
k_{AV} (min^{-1})	Avrami-fractional-order rate constant
k_1 (min^{-1})	Pseudo-first-order rate constant
k_2 (g mg^{-1} min^{-1})	Pseudo-second-order rate constant
k_{id} (mg g^{-1} min^{-1})	Intraparticle diffusion constant
n_{AV}	Avrami fractional order related to the adsorption mechanism
α (mg (g^{-1} min^{-1}))	Initial rate adsorption
β (mg g^{-1})	Related to the activation energy and surface coverage
C (mg g^{-1})	Constant connected to the boundary layer
K_L (L mg^{-1})	BET constant of multilayer adsorption
K_F (mg g^{-1}(mg L^{-1})$^{-1/n}$)	Freundlich adsorption constant
K_S (L mg^{-1})	BET, Langmuir and Sips constant of monolayer adsorption
n_F	Constant depicting adsorption intensity
n_S	Sips exponent
R^2	Correlation coefficient
R^2_{adj}	Adjusted correlation coefficient
SSE	Sum of square errors
HYBIRD	Hybrid fractional error
$\Delta H°$ (J mol^{-1})	Enthalpy change
$\Delta G°$ (kJ mol^{-1})	Gibbs free energy
$\Delta S°$ (J mol^{-1} K^{-1})	Entropy change

References

1. Adebayo MA, Prola LDT, Lima EC et al (2014) Adsorption of Procion Blue MX-R dye from aqueous solutions by lignin chemically modified with aluminium and manganese. J Hazard Mater 268:43–50. https://doi.org/10.1016/j.jhazmat.2014.01.005
2. Ahmad MA, Mohamad Yusop MF, Zakaria R et al (2021) Adsorption of methylene blue from aqueous solution by peanut shell based activated carbon. Mater Today Proc. https://doi.org/10.1016/j.matpr.2021.02.789
3. Alencar WS, Lima EC, Royer B et al (2012) Application of Aqai Stalks as Biosorbents for the Removal of the Dye Procion Blue MX-R from Aqueous Solution. Sep Sci Technol 47:513–526. https://doi.org/10.1080/01496395.2011.616568
4. An FQ, Wu RY, Li M et al (2017) Adsorption of heavy metal ions by iminodiacetic acid functionalized D301 resin: Kinetics, isotherms and thermodynamics. React Funct Polym 118:42–50. https://doi.org/10.1016/j.reactfunctpolym.2017.07.005
5. Anastas PT, Zimmerman JB (2003) Design through the 12 principles of green engineering. Environ Sci Technol 37. https://doi.org/10.1021/es032373g. :94A-101A
6. Babalola JO, Koiki BA, Eniayewu Y et al (2016) Adsorption efficacy of Cedrela odorata seed waste for dyes: Nonlinear fractal kinetics and nonlinear equilibrium studies. J Environ Chem Eng 4:3527–3536. https://doi.org/10.1016/j.jece.2016.07.027
7. Barrer RM (1966) Specificity in physical sorption. J Colloid Interface Sci 21:415–434. https://doi.org/10.1016/0095-8522(66)90007-9
8. Barrett EP, Joyner LG, Halenda PP (1951) The determination of pore volume and area distributions in porous substances. J Am Chem Soc 73:373–380. https://doi.org/10.1021/ja01145a126
9. Barton SS (1987) The adsorption of methylene blue by active carbon. Carbon N Y 25:343–350. https://doi.org/10.1016/0008-6223(87)90005-4
10. Basu S, Ghosh G, Saha S (2018) Adsorption characteristics of phosphoric acid induced activation of bio-carbon: Equilibrium, kinetics, thermodynamics and batch adsorber design. Process Saf Environ Prot 117:125–142. https://doi.org/10.1016/j.psep.2018.04.015
11. Brunauer S, Emmett PH, Teller E (1938) Adsorption of gases in multimolecular layers. J Am Chem Soc 60:309–319. https://doi.org/10.1021/ja01269a023
12. Calimli MH, Nas MS, Burhan H et al (2020) Preparation, characterization and adsorption kinetics of methylene blue dye in reduced-graphene oxide supported nanoadsorbents. J Mol Liq 309:113171. https://doi.org/10.1016/j.molliq.2020.113171
13. Carvalho C, de O, Rodrigues DLC, Lima ÉC et al (2019) Kinetic, equilibrium, and thermodynamic studies on the adsorption of ciprofloxacin by activated carbon produced from Jerivá (*Syagrus romanzoffiana*). Environ Sci Pollut Res 26:4690–4702. https://doi.org/10.1007/s11356-018-3954-2
14. Coimbra MC, Jorge N (2011) Proximate composition of guariroba (*Syagrus oleracea*), jerivá (*Syagrus romanzoffiana*) and macaúba (*Acrocomia aculeata*) palm fruits. Food Res Int 44:2139–2142.

https://doi.org/10.1016/j.foodres.2011.03.032

15. Cremasco MA (2015) Fundamentos de transferência de massa, 3rd edn. Blucher, São Paulo
16. Danish M, Ahmad T, Hashim R et al (2018) Comparison of surface properties of wood biomass activated carbons and their application against rhodamine B and methylene blue dye. Surfaces and Interfaces 11:1–13. https://doi.org/10.1016/j.surfin.2018.02.001
17. Dawood S, Sen TK, Phan C (2017) Synthesis and characterization of slow pyrolysis pine cone bio-char in the removal of organic and inorganic pollutants from aqueous solution by adsorption: Kinetic, equilibrium, mechanism and thermodynamic. Bioresour Technol 246:76–81. https://doi.org/10.1016/j.biortech.2017.07.019
18. Dawood S, Sen TK, Phan C (2016) Adsorption removal of Methylene Blue (MB) dye from aqueous solution by bio-char prepared from *Eucalyptus sheathiana* bark: kinetic, equilibrium, mechanism, thermodynamic and process design. Desalin Water Treat 57:28964–28980. https://doi.org/10.1080/19443994.2016.1188732
19. de Costa PD, Furmanski LM, Dominguini L (2015) Production, characterization and application of activated carbon from nutshell for adsorption of methylene blue. Rev Virtual Quim 7:1272–1285. https://doi.org/10.5935/1984-6835.20150070
20. de Sales PF, Bertoli AC, Pinto FM, Magriotis ZM (2015) Production, characterization and application of activated carbon obtained from the corncob: The search for the reuse of an agroindustrial waste. Rev Virtual Quim 7:1174–1188. https://doi.org/10.5935/1984-6835.20150066
21. Deng H, Li G, Yang H et al (2010) Preparation of activated carbons from cotton stalk by microwave assisted KOH and K2CO3 activation. Chem Eng J 163:373–381. https://doi.org/10.1016/j.cej.2010.08.019
22. dias Júnior AF, de Oliveira RN, Deglise X et al (2019) Infrared spectroscopy analysis on charcoal generated by the pyrolysis of Corymbia citriodora wood. Rev Mater 24:1–7. https://doi.org/10.1590/s1517-707620190003.0700
23. Doğan M, Alkan M, Türkyilmaz A, Özdemir Y (2004) Kinetics and mechanism of removal of methylene blue by adsorption onto perlite. J Hazard Mater 109:141–148. https://doi.org/10.1016/j.jhazmat.2004.03.003
24. Enniya I, Rghioui L, Jourani A (2018) Adsorption of hexavalent chromium in aqueous solution on activated carbon prepared from apple peels. Sustain Chem Pharm 7:9–16. https://doi.org/10.1016/j.scp.2017.11.003
25. Falasca SL, Miranda Del Fresno C, Ulberich A (2012) Possibilities for growing queen palm (*Syagrus romanzoffiana*) in Argentina as a biodiesel producer under semi-arid climate conditions. Int J Hydrogen Energy 37:14843–14848. https://doi.org/10.1016/j.ijhydene.2011.12.092
26. Feng Y, Yang F, Wang Y et al (2011) Basic dye adsorption onto an agro-based waste material - Sesame hull (*Sesamum indicum* L.). Bioresour Technol 102:10280–10285. https://doi.org/10.1016/j.biortech.2011.08.090

27. Feng Y, Zhou H, Liu G et al (2012) Methylene blue adsorption onto swede rape straw (Brassica napus L.) modified by tartaric acid: Equilibrium, kinetic and adsorption mechanisms. Bioresour Technol 125:138–144. https://doi.org/10.1016/j.biortech.2012.08.128
28. Freundlich H (1906) Adsorption in solution. J Phys Chem 40:1361–1368
29. Gupta M, Gupta H, Kharat DS (2018) Adsorption of Cu(II) by low cost adsorbents and the cost analysis. Environ Technol Innov 10:91–101. https://doi.org/10.1016/j.eti.2018.02.003
30. Hameed BH, Ahmad AA (2009) Batch adsorption of methylene blue from aqueous solution by garlic peel, an agricultural waste biomass. J Hazard Mater 164:870–875. https://doi.org/10.1016/j.jhazmat.2008.08.084
31. Han Q, Wang J, Goodman BA et al (2020) High adsorption of methylene blue by activated carbon prepared from phosphoric acid treated eucalyptus residue. Powder Technol 366:239–248. https://doi.org/10.1016/j.powtec.2020.02.013
32. Hasan R, Chong CC, Setiabudi HD et al (2019) Process optimization of methylene blue adsorption onto eggshell–treated palm oil fuel ash. Environ Technol Innov 13:62–73. https://doi.org/10.1016/j.eti.2018.10.004
33. Ho YS, McKay G (1998) The kinetics of sorption of basic dyes from aqueous solution by sphagnum moss peat. Can J Chem Eng 76:822–827. https://doi.org/10.1002/cjce.5450760419
34. Hou J, Chen Y, Shi W et al (2020) Graphene oxide/methylene blue composite membrane for dyes separation: Formation mechanism and separation performance. Appl Surf Sci 505:144145. https://doi.org/10.1016/j.apsusc.2019.144145
35. Iwuozor KO, Ighalo JO, Ogunfowora LA et al (2021) An empirical literature analysis of adsorbent performance for methylene blue uptake from aqueous media. J Environ Chem Eng 9:105658. https://doi.org/10.1016/j.jece.2021.105658
36. Jawad AH, Saud Abdulhameed A, Wilson LD et al (2021) High surface area and mesoporous activated carbon from KOH-activated dragon fruit peels for methylene blue dye adsorption: Optimization and mechanism study. Chinese J Chem Eng 32:281–290. https://doi.org/10.1016/j.cjche.2020.09.070
37. Karagöz S, Tay T, Ucar S, Erdem M (2008) Activated carbons from waste biomass by sulfuric acid activation and their use on methylene blue adsorption. Bioresour Technol 99:6214–6222. https://doi.org/10.1016/j.biortech.2007.12.019
38. Kavitha D, Namasivayam C (2007) Experimental and kinetic studies on methylene blue adsorption by coir pith carbon. Bioresour Technol 98:14–21. https://doi.org/10.1016/j.biortech.2005.12.008
39. Kebede TG, Mengistie AA, Dube S et al (2018) Study on adsorption of some common metal ions present in industrial effluents by Moringa stenopetala seed powder. J Environ Chem Eng 6:1378–1389. https://doi.org/10.1016/j.jece.2018.01.012
40. Lagergreen S (1898) Zur theorie der sogenannten adsorption gelöster stoffe. K Sven Vetenskapsakademiens 24:1–39

41. Lammers K, Arbuckle-Keil G, Dighton J (2009) FT-IR study of the changes in carbohydrate chemistry of three New Jersey pine barrens leaf litters during simulated control burning. Soil Biol Biochem 41:340–347. https://doi.org/10.1016/j.soilbio.2008.11.005
42. Langmuir I (1918) The Adsorption of Gases on Glass, Mica and Platinum. the Adsorption of Gases on Plane Surfaces of Glass, Mica and Platinum. J Am Chem Soc 345:1361–1368
43. Lima ÉC, Adebayo MA, Machado FM (2015) Kinetic and Equilibrium Models of Adsorption. In: Bergmann CP, Machado FM (reds) Carbon Nanomaterials as Adsorbents for Environmental and Biological Applications, 1st edn. Springer, New York, bll 33–71
44. Lima EC, Cestari AR, Adebayo MA (2016) Comments on the paper: a critical review of the applicability of Avrami fractional kinetic equation in adsorption-based water treatment studies. Desalin Water Treat 57:19566–19571. https://doi.org/10.1080/19443994.2015.1095129
45. Liu QS, Zheng T, Wang P et al (2010) Adsorption isotherm, kinetic and mechanism studies of some substituted phenols on activated carbon fibers. Chem Eng J 157:348–356. https://doi.org/10.1016/j.cej.2009.11.013
46. Liu T, Li Y, Du Q et al (2012) Adsorption of methylene blue from aqueous solution by graphene. Colloids Surfaces B Biointerfaces 90:197–203. https://doi.org/10.1016/j.colsurfb.2011.10.019
47. Liu W-J, Zeng F-X, Jiang H, Zhang X-S (2011) Preparation of high adsorption capacity bio-chars from waste biomass. Bioresour Technol 102:8247–8252. https://doi.org/10.1016/j.biortech.2011.06.014
48. Liu Y, Liu Y-J (2008) Biosorption isotherms, kinetics and thermodynamics. Sep Purif Technol 61:229–242. https://doi.org/10.1016/j.seppur.2007.10.002
49. Lopes ECN, Dos Anjos FSC, Vieira EFS, Cestari AR (2003) An alternative Avrami equation to evaluate kinetic parameters of the interaction of Hg(II) with thin chitosan membranes. J Colloid Interface Sci 263:542–547. https://doi.org/10.1016/S0021-9797(03)00326-6
50. Luo H, Huang X, Luo Y et al (2018) Adsorption behavior and mechanism of acidic blue 25 dye onto cucurbit[8]uril: A spectral and DFT study. Spectrochim Acta - Part A Mol Biomol Spectrosc 193:125–132. https://doi.org/10.1016/j.saa.2017.12.006
51. Mahmoodi NM, Arami M, Bahrami H, Khorramfar S (2010) Novel biosorbent (*Canola hull*): Surface characterization and dye removal ability at different cationic dye concentrations. Desalination 264:134–142. https://doi.org/10.1016/j.desal.2010.07.017
52. Medhat A, El-Maghrabi HH, Abdelghany A et al (2021) Efficiently activated carbons from corn cob for methylene blue adsorption. Appl Surf Sci Adv 3:100037. https://doi.org/10.1016/j.apsadv.2020.100037
53. Molina-Sabio M, Rodríguez-Reinoso F (2004) Role of chemical activation in the development of carbon porosity. Colloids Surfaces A Physicochem Eng Asp 241:15–25. https://doi.org/10.1016/j.colsurfa.2004.04.007
54. Moreira MAC, Payret Arrúa ME, Antunes AC et al (2013) Characterization of Syagrus romanzoffiana oil aiming at biodiesel production. Ind Crops Prod 48:57–60. https://doi.org/10.1016/j.indcrop.2013.04.006

55. Nascimento RF, de Lima ACA, Vidal CB et al (2014) Adsorção: Aspectos teóricos e aplicações ambientais
56. NCBI - National Center of Biotechnology Information (2020) Methylene blue, CID 6099. In: PubChem Database
57. Othman NH, Alias NH, Shahruddin MZ et al (2018) Adsorption Kinetics of Methylene Blue Dyes onto Magnetic Graphene Oxide. J Environ Chem Eng 6:2803–2811. https://doi.org/10.1016/j.jece.2018.04.024
58. Özcan AS, Erdem B, Özcan A (2005) Adsorption of Acid Blue 193 from aqueous solutions onto BTMA-bentonite. Colloids Surfaces A Physicochem Eng Asp 266:73–81. https://doi.org/10.1016/j.colsurfa.2005.06.001
59. Özgenç Ö, Durmaz S, Boyaci IH, Eksi-Kocak H (2017) Determination of chemical changes in heat-treated wood using ATR-FTIR and FT Raman spectrometry. Spectrochim Acta - Part A Mol Biomol Spectrosc 171:395–400. https://doi.org/10.1016/j.saa.2016.08.026
60. Pan X, Cheng S, Su T et al (2019) Fenton-like catalyst Fe_3O_4@polydopamine-MnO_2 for enhancing removal of methylene blue in wastewater. Colloids Surfaces B Biointerfaces 181:226–233. https://doi.org/10.1016/j.colsurfb.2019.05.048
61. Parakala S, Moulik S, Sridhar S (2019) Effective separation of methylene blue dye from aqueous solutions by integration of micellar enhanced ultrafiltration with vacuum membrane distillation. Chem Eng J 375:122015. https://doi.org/10.1016/j.cej.2019.122015
62. Pérez-Marín AB, Zapata VM, Ortuño JF et al (2007) Removal of cadmium from aqueous solutions by adsorption onto orange waste. J Hazard Mater 139:122–131. https://doi.org/10.1016/j.jhazmat.2006.06.008
63. Pigatto J, Brandler D, Tochetto G et al (2020) Development and characterization of a new adsorbent based on Jerivá coconut (*Syagrus romanzoffiana*) applied for removing toxic metals from water. Desalin Water Treat 201:267–277. https://doi.org/10.5004/dwt.2020.25893
64. Pintor AMA, Silvestre-Albero AM, Ferreira CIA et al (2013) Textural and Surface Characterization of Cork-Based Sorbents for the Removal of Oil from Water. Ind Eng Chem Res 52:16427–16435. https://doi.org/10.1021/ie402038n
65. Prajapati AK, Mondal MK (2020) Comprehensive kinetic and mass transfer modeling for methylene blue dye adsorption onto CuO nanoparticles loaded on nanoporous activated carbon prepared from waste coconut shell. J Mol Liq 307:112949. https://doi.org/10.1016/j.molliq.2020.112949
66. Ruthven DM (1984) Principles of Adsorption and Adsorption processes
67. Salomón YLDO, Georgin J, Franco DSP et al (2021) High-performance removal of 2,4-dichlorophenoxyacetic acid herbicide in water using activated carbon derived from Queen palm fruit endocarp (*Syagrus romanzoffiana*). J Environ Chem Eng 9:104911. https://doi.org/10.1016/j.jece.2020.104911
68. Sellaoui L, Franco D, Ghalla H et al (2020) Insights of the adsorption mechanism of methylene blue on brazilian berries seeds: Experiments, phenomenological modelling and DFT calculations. Chem

Eng J 394:125011. https://doi.org/10.1016/j.cej.2020.125011

69. Selmi T, Enaime G, Kesraoui A et al (2021) Dye removal by activated carbon produced from Agave americana fibers: stochastic isotherm and fractal kinetic studies. Environ Sci Pollut Res 28:46580–46591. https://doi.org/10.1007/s11356-020-10768-2
70. Setiabudi HD, Jusoh R, Suhaimi SFRM, Masrur SF (2016) Adsorption of methylene blue onto oil palm (*Elaeis guineensis*) leaves: Process optimization, isotherm, kinetics and thermodynamic studies. J Taiwan Inst Chem Eng 63:363–370. https://doi.org/10.1016/j.jtice.2016.03.035
71. Sips R (1950) On the structure of a catalyst surface. J Chem Phys 18:1024–1026. https://doi.org/10.1063/1.1747848
72. Somsesta N, Sricharoenchaikul V, Aht-Ong D (2020) Adsorption removal of methylene blue onto activated carbon/cellulose biocomposite films: Equilibrium and kinetic studies. Mater Chem Phys 240:122221. https://doi.org/10.1016/j.matchemphys.2019.122221
73. Subratti A, Vidal JL, Lalgee LJ et al (2021) Preparation and characterization of biochar derived from the fruit seed of *Cedrela odorata* L and evaluation of its adsorption capacity with methylene blue. Sustain Chem Pharm 21:100421. https://doi.org/10.1016/j.scp.2021.100421
74. Tang Y, Zhao Y, Lin T et al (2019) Adsorption performance and mechanism of methylene blue by H_3PO_4- modified corn stalks. J Environ Chem Eng 7:103398. https://doi.org/10.1016/j.jece.2019.103398
75. Thi HT, Hoang A, Le, Huu TP et al (2020) Adsorption isotherms and kinetics modeling of methylene blue dye onto a carbonaceous hydrochar adsorbent derived from coffe husk waste. Sci Total Environ 725:138325. https://doi.org/10.1016/j.scitotenv.2020.138325
76. Thommes M, Kaneko K, Neimark AV et al (2015) Physisorption of gases, with special reference to the evaluation of surface area and pore size distribution (IUPAC Technical Report). Pure Appl Chem 87:1051–1069. https://doi.org/10.1515/pac-2014-1117
77. Wang H, Xie R, Zhang J, Zhao J (2018) Preparation and characterization of distillers' grain based activated carbon as low cost methylene blue adsorbent: Mass transfer and equilibrium modeling. Adv Powder Technol 29:27–35. https://doi.org/10.1016/j.apt.2017.09.027
78. Wang J, Chen B (2015) Adsorption and coadsorption of organic pollutants and a heavy metal by graphene oxide and reduced graphene materials. Chem Eng J 281:379–388. https://doi.org/10.1016/j.cej.2015.06.102
79. Weber WJ, Morris JC (1963) Kinetics of adsorption carbon from solutions. J Sanit Engeering Div Proc 89:31–60
80. Weng CH, Lin YT, Tzeng TW (2009) Removal of methylene blue from aqueous solution by adsorption onto pineapple leaf powder. J Hazard Mater 170:417–424. https://doi.org/10.1016/j.jhazmat.2009.04.080
81. Yağmur HK, Kaya İ (2021) Synthesis and characterization of magnetic ZnCl2-activated carbon produced from coconut shell for the adsorption of methylene blue. J Mol Struct 1232:130071. https://doi.org/10.1016/j.molstruc.2021.130071

82. Yuvaraja G, Krishnaiah N, Subbaiah MV, Krishnaiah A (2014) Biosorption of Pb(II) from aqueous solution by Solanum melongena leaf powder as a low-cost biosorbent prepared from agricultural waste. Colloids Surfaces B Biointerfaces 114:75–81. https://doi.org/10.1016/j.colsurfb.2013.09.039
83. Yuvaraja G, Krishnaiah N, Subbaiah MV, Krishnaiah A (2014) Biosorption of Pb(II) from aqueous solution by Solanum melongena leaf powder as a low-cost biosorbent prepared from agricultural waste. Colloids Surfaces B Biointerfaces 114:75–81. https://doi.org/10.1016/j.colsurfb.2013.09.039

Figures

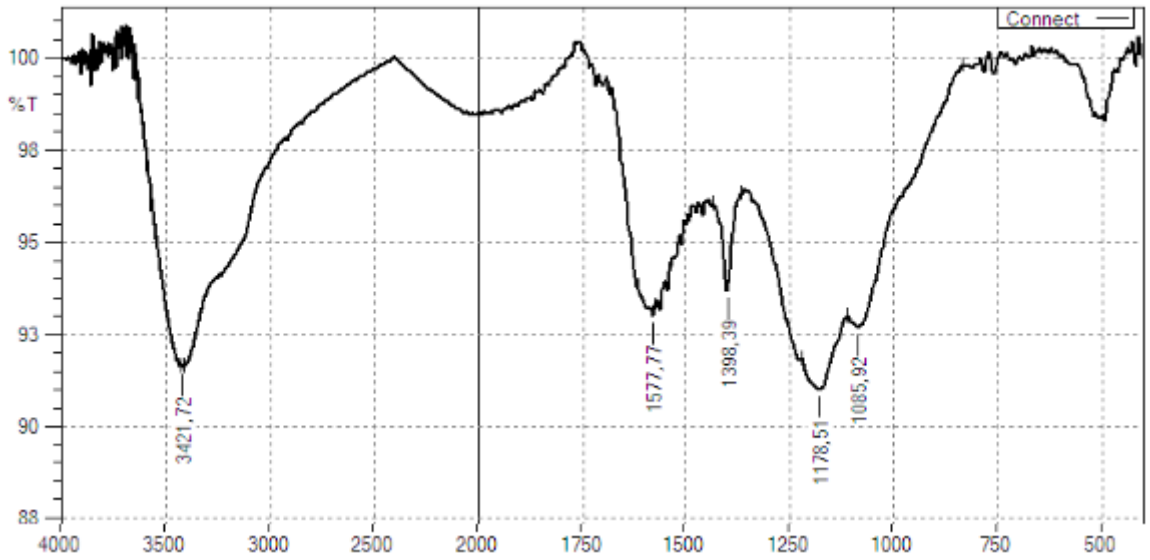

Figure 1

Infrared spectrum obtained by FTIR for ACJC

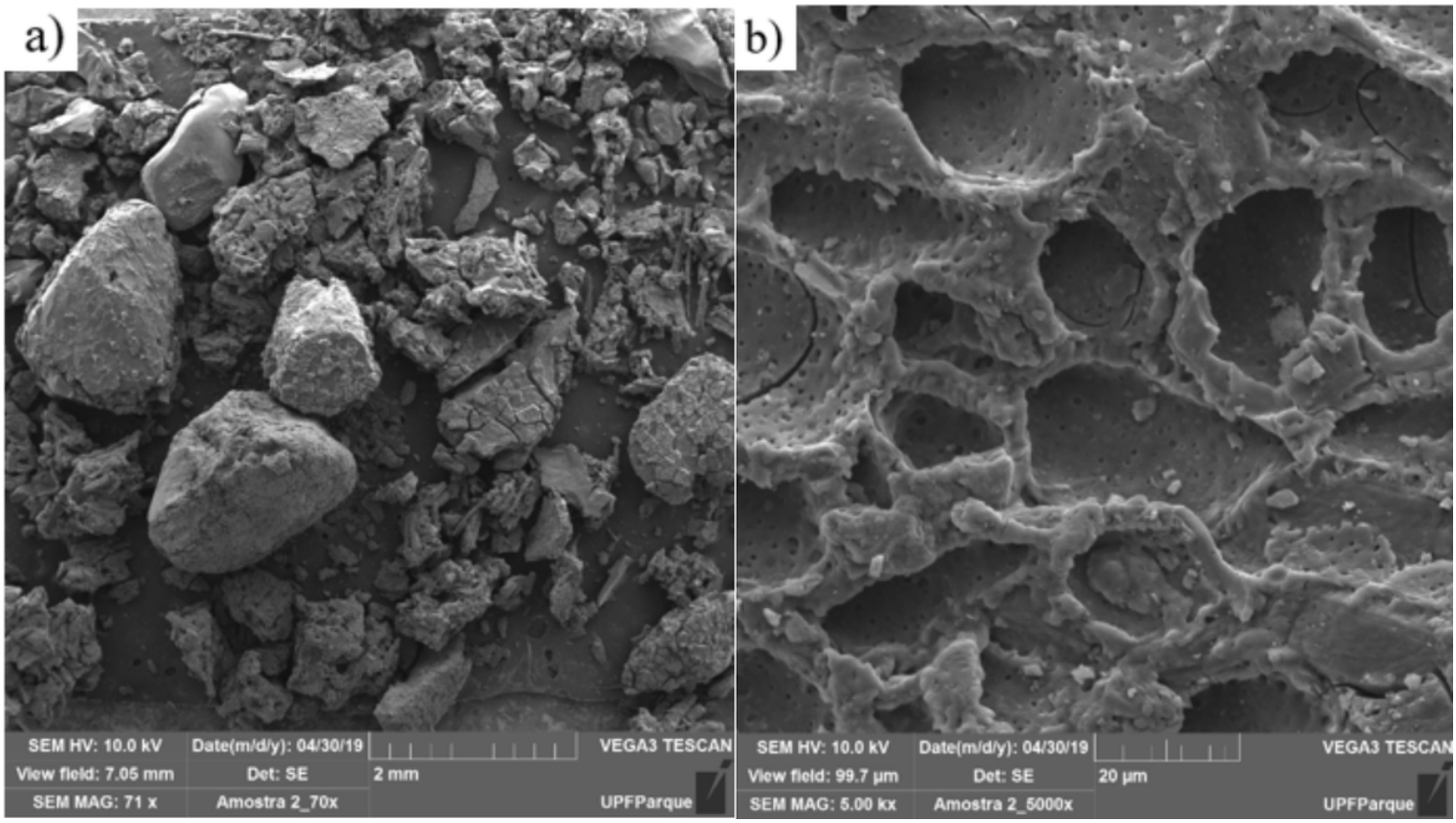

Figure 2

Isolated SEM micrographs of ACJC at magnifications of 70 (a) and 5000 times (b).

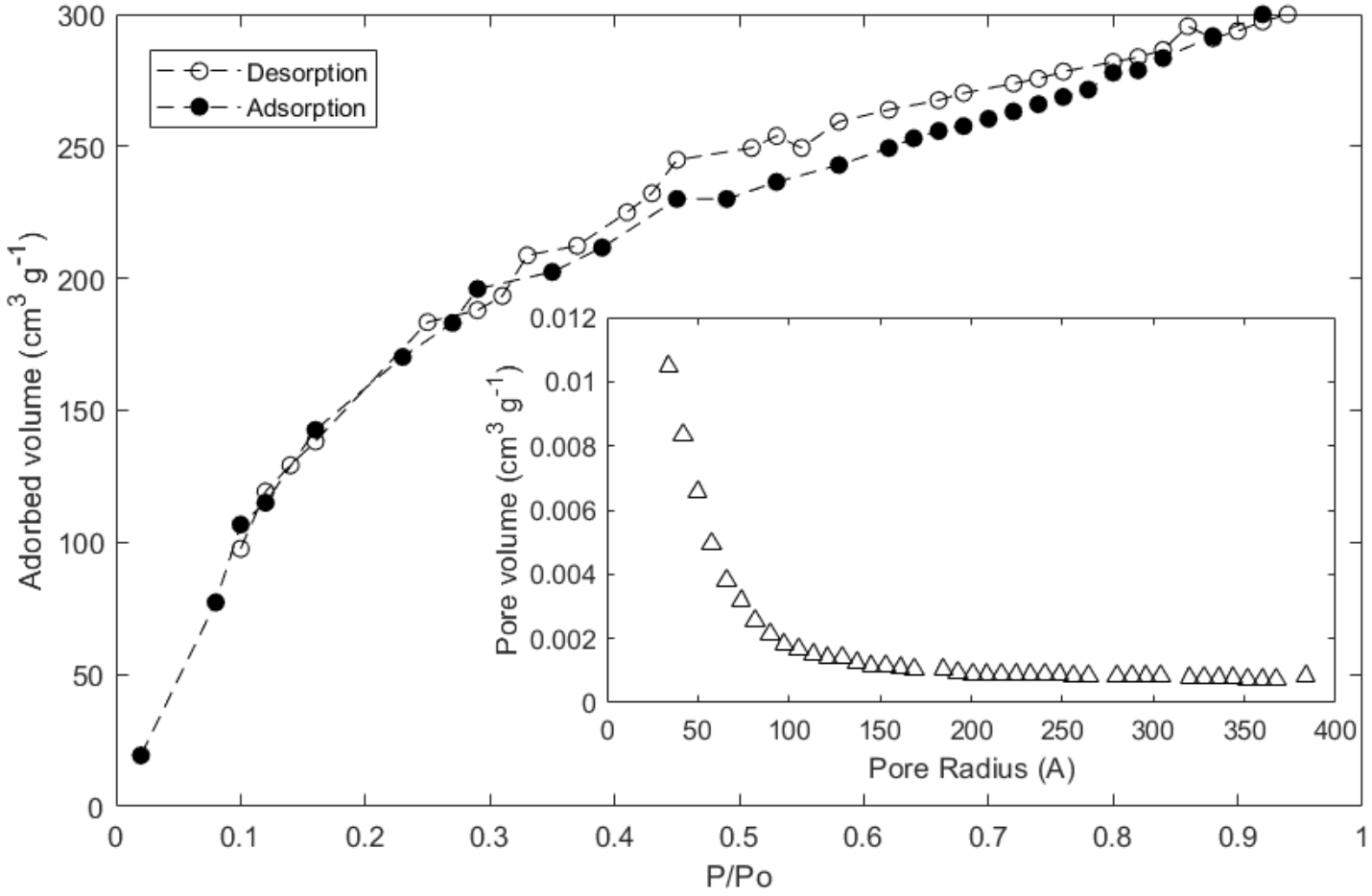

Figure 3

Volume of N2 adsorbed/desorbed versus relative pressure of activated carbon.

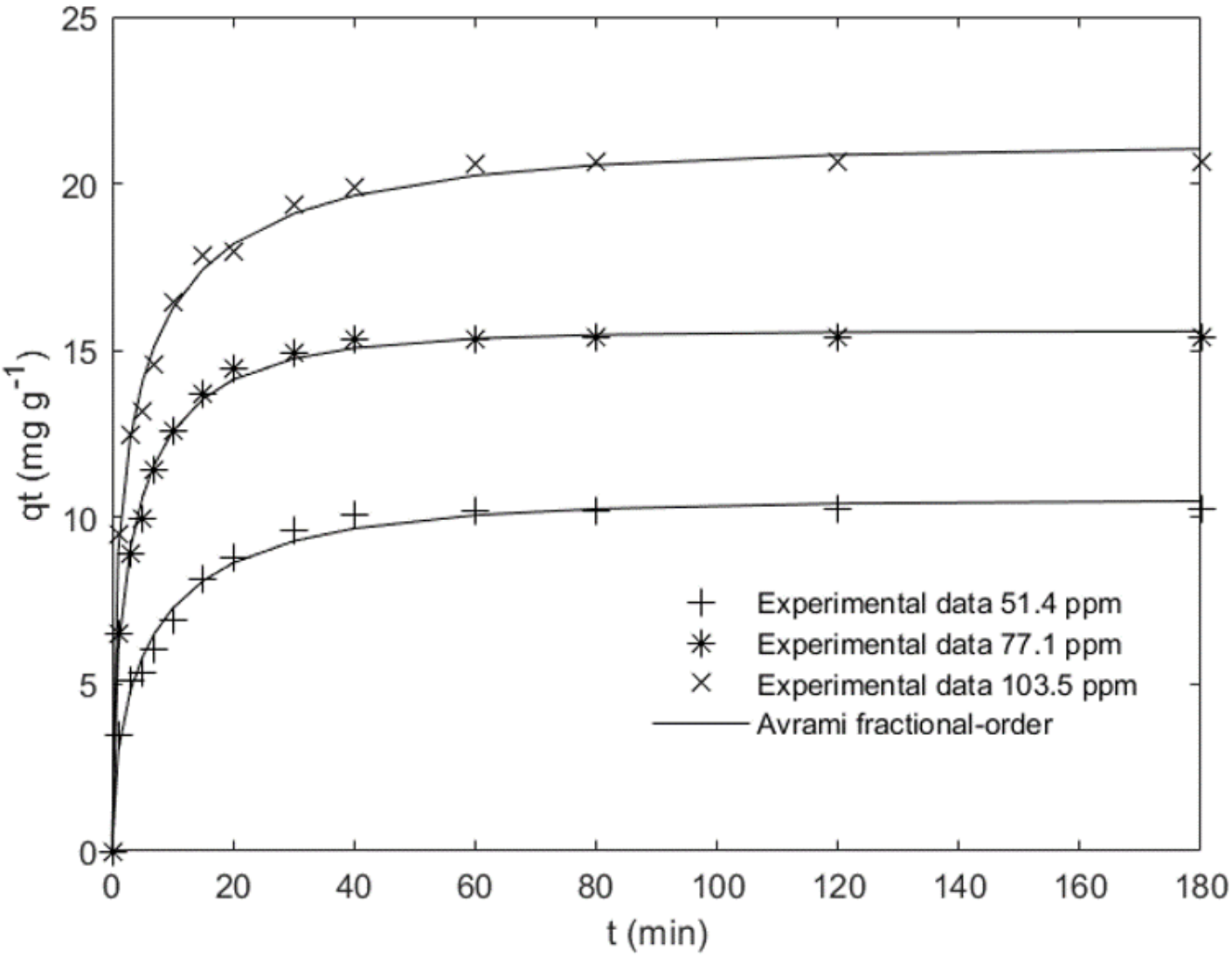

Figure 4

Kinetic adsorption curves for MB on ACJC fitted to the Avrami fractional-order model (T = 298 K, adsorbent dosage = 5 g L-1, shaking = 150 rpm, pHi = 5.85, pHf = 2.44).

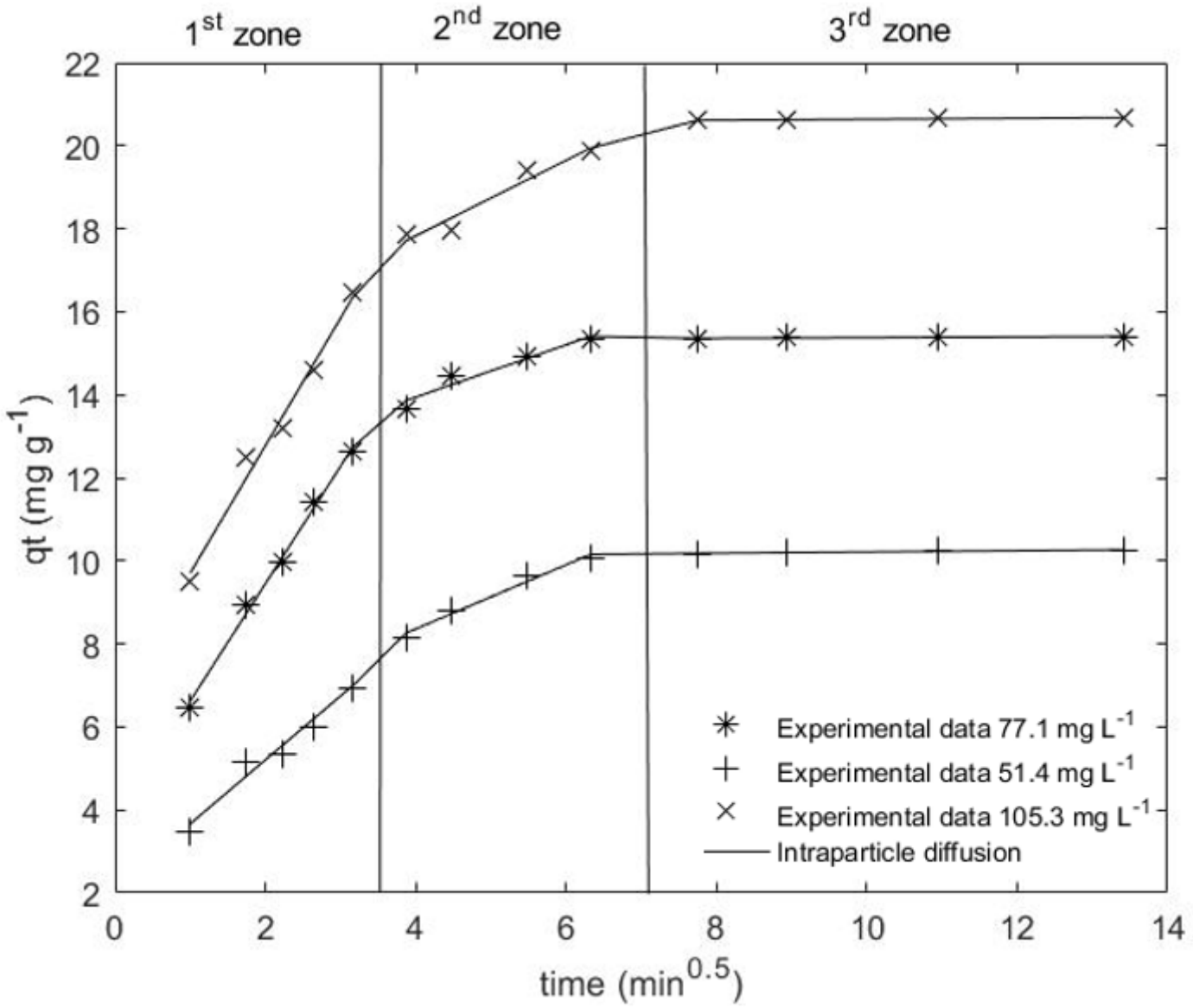

Figure 5

Intraparticle diffusion kinetics for MB on ACJC (T = 298 K, adsorbent dosage = 5 g L-1, shaking = 150 rpm, pHi = 5.85, pHf = 2.44).

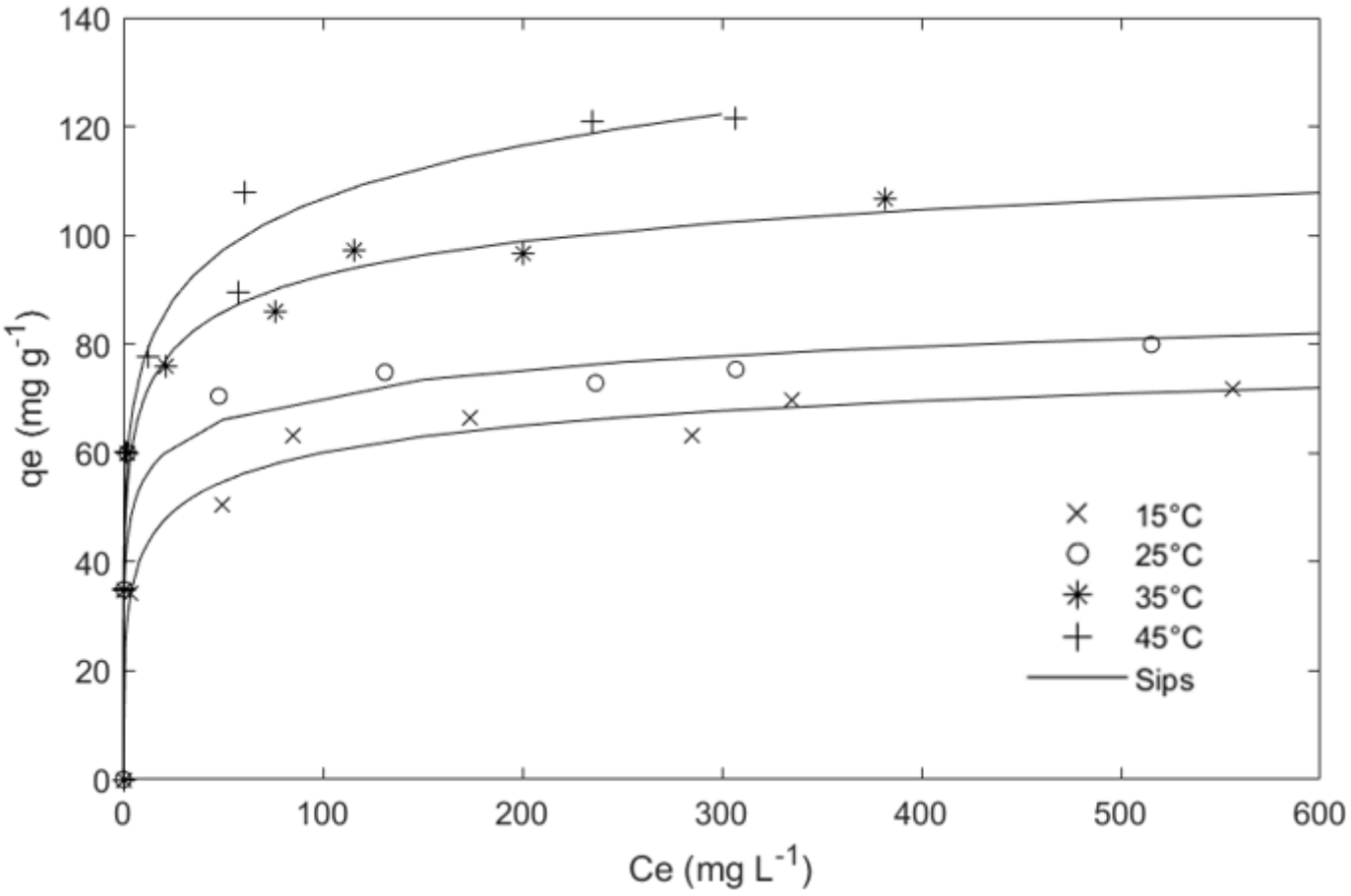

Figure 6

Isotherm adsorption curves for MB on ACJC fitted to the Sips model (adsorbent dosage = 5 g L-1, shaking = 150 rpm, pHi = 5.85, pHf = 2.44).

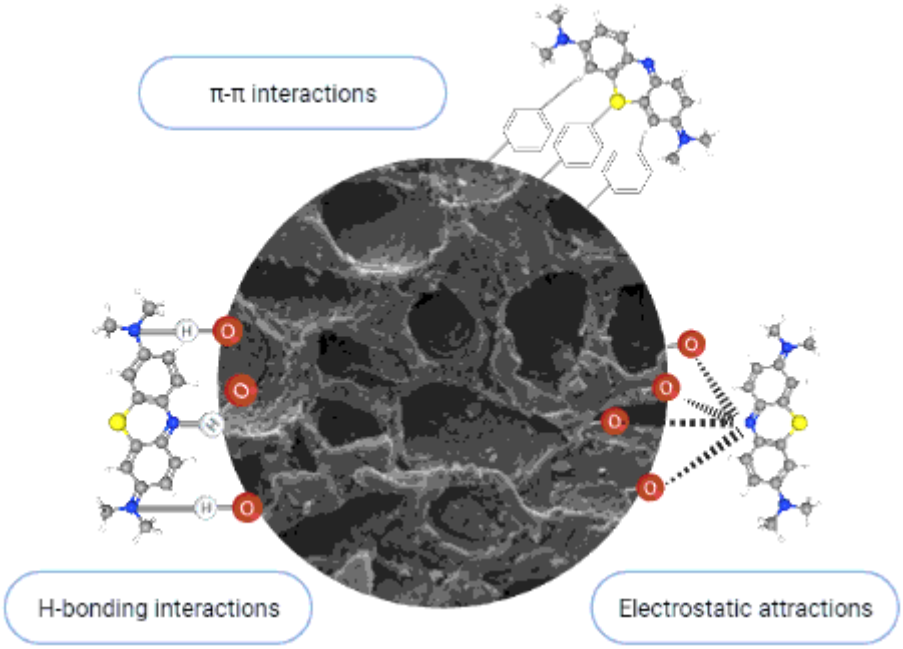

Figure 7

Illustration of the possible interactions between MB and the functional groups on the surface of ACJC.

Supplementary Files

This is a list of supplementary files associated with this preprint. Click to download.

- Supplementarymaterial.docx